DFT Research on the Dehydroxylation Reaction of Pyrophyllite 1. First-Principle Molecular Dynamics Simulations

Esther Molina-Montes,[†] Davide Donadio,[‡] Alfonso Hernández-Laguna,[§] C. Ignacio Sainz-Díaz,*[,†] and Michele Parrinello[‡]

Laboratorio de Estudios Cristalográficos, Instituto Andaluz de Ciencias de la Tierra (CSIC), UniVersidad de Granada, AV. FuentenueVa s/n, 18002-Granada, Spain, Laboratory of Physical Chemistry, ETH Zurich, USI Campus, Via Giuseppe Buffi 13, CH-6904 Lugano, Switzerland, and Estación Experimental del Zaidín (CSIC), C/ Profesor Albareda 1, 18008-Granada, Spain

The dehydroxylation of pyrophyllite involves the reaction of OH groups and elimination of water molecules through two possible mechanisms, one involving the bridging hydroxyl groups of an octahedral Al^{3+} pair and the other two hydroxyl groups reacting across the dioctahedral vacancy. First-principles molecular dynamics simulations at the density functional theory level are used together with the metadynamics algorithm to explore the free-energy surface (FES) of the initial step of the dehydroxylation. We observe that the two possible dehydroxylation mechanisms yield similar activation energies at 0 K, but at high temperatures, the cross mechanism has lower free energy than that of the on-site one. The dehydroxylation process produces different semidehydroxylated intermediates that should be taken into account. The role of the temperature in favoring a dehydroxylation nonconcerted chain mechanism over another is here elucidated, and a novel competitive mechanism, which is assisted by the structural apical oxygens in the high-temperature regime, is proposed.

Introduction

Pyrophyllite is a classical model for dioctahedral 2:1 phyllosilicates that consists of a layered structure containing an aluminum octahedral sheet sandwiched between two silicon tetrahedral sheets. The octahedral sheet is bonded to the tetrahedral ones by apical structural oxygen atoms, and the six-fold coordination of the aluminum atoms is completed by −OH groups (Figure 1a). In the dioctahedral phyllosilicate, only two of the possible octahedral cation sites are filled up, and one octahedral hole per unit cell remains.

The high-temperature transformations of phyllosilicates play an important role in ceramic technology, in the design of new materials, such as resins, plastics and paints, in chemical and nuclear waste management, as well as in geological processes related to sediment overpressurization and continental margins. Particularly, the hydration and dehydration reactions of clays are important in many geological processes and have been linked to phenomena of diverse sediments overpressuring and petroleum diffusion[1,2] and the smectite to illite transition.[1–3] To achieve a better understanding of the thermally induced degradation process of phyllosilicates, it is necessary to explore these mechanisms at an atomistic level, so as to discover the underlying processes and design new ones. The study of these phenomena is also functional to several industrial applications which involve thermal treatments that produce big changes in the physical−chemical properties of clay minerals.

Pyrophyllite is a widely studied paradigm within this class of minerals, as it has a relatively simple structure and displays the typical behavior of dioctahedral clays upon heating; namely, dehydroxylation occurs between 500 and 900 °C, while above 900 °C, amorphization takes place.[4] The dehydroxylation of pyrophyllite involves the reaction of the OH groups which link the aluminum cations in the octahedral sheet, yielding the formation of one water molecule per half unit cell (Figure 1b). This process leads to the formation of a dehydroxylate phase, which has been characterized by nuclear magnetic resonance (NMR),[5] powder X-ray diffraction (XRD),[6] and infrared spectroscopy.[7] Pyrophyllite dehydroxylate (Figure 1b) consists of five-coordinated, distorted, trigonal bipyramidal AlO_5 units in the octahedral sheet, sandwiched between distorted but intact tetrahedral SiO_4 sheets, where the residual oxygen left behind sits between the two remaining aluminum cations.[8–10] The dehydroxylation reaction is completed when the water molecule migrates out of the octahedral hole and is released throughout the interlaminar space.

In earlier studies, two possible dehydroxylation mechanisms have been suggested; one involves the OH groups oriented toward the same octahedral hole across the octahedral vacant,[11,12] and the other involves the two OH groups situated on an edge-sharing pair of aluminum octahedrons and oriented toward different holes.[8] In this work, we name these mechanisms as cross and on-site mechanisms, respectively. Spectroscopic studies revealed also the occurrence of an intermediate partially dehydroxylated phase,[7,13] the structure of which was proposed in a recent theoretical quantum mechanical study as a semidehydroxylate phase.[14] In addition, structures containing residual SiOH groups have been revealed by IR spectroscopy,[15] suggesting the occurrence of other possible intermediate structures.

Recently, the structures of pyrophyllite and of other clay minerals have been investigated by first-principles calculations that have reproduced the diffraction patterns and the vibrational spectra.[16,17] DFT calculations on periodic models have defined a series of intermediates for the dehydroxylation process of pyrophyllite.[14] At this level of theory, cis-vacant and trans-vacant configurations of pyrophyllite have been examined in order to explain the different thermal behavior, structural

transformations, and energetics of the dehydroxylation reaction.[18]

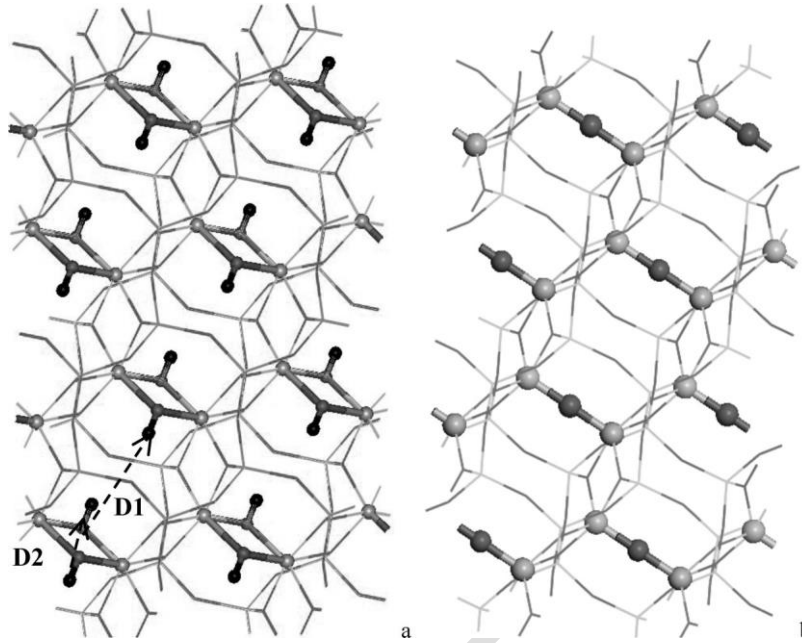

Figure 1. Structure of pyrophyllite (a) and the dehydroxylate derivative (b, on the left). D1 and D2 are the (H ··· O) distances employed as CVs. The atoms that participate directly in the reaction are represented with balls; Al (clear grey), O (grey), and H (black).

In the present work, we apply Car−Parrinello molecular dynamics (CPMD)[19,20] to study the mechanism and the thermodynamics of the dehydroxylation reaction of pyrophyllite. This method, combined with the metadynamics algorithm,[21,22] allows for an efficient study of complex processes in solid-state systems and an estimation of the free-energy profiles.[23,24] The formation of the semidehydroxylated structures is also studied in order to identify the intermediates in the actual reaction mechanism among the ones proposed and to investigate the possible formation of other unpredicted intermediate structures.

Models and Methods

We perform-first principles calculations using the density functional theory (DFT)[25] in the generalized gradient approximation (GGA) with the BLYP parametrization for the exchange−correlation functional.[26,27] The Kohn−Sham orbitals are expanded in a plane-wave basis set up to an energy cutoff of 70 Ry. In this work, we use norm-conserving Troullier Martin pseudopotentials to describe the interaction between the valence electrons and the core.[28] Ab initio Car−Parrinello MD simulations[19] are performed with a time step of 0.12 fs and fictitious electron mass of 800 au in the constant volume and constant energy (NVE) ensemble. The CPMD package (CPMD v.3.9) is used.[29]

The dehydroxylation of pyrophyllite is a thermally activated reaction with different pathways. Previous static calculations of this reaction[14,18] and our preliminary MD simulations indicate that the exploration of this reaction would not be observed within the time of several picoseconds, which is currently accessible to a first-principle MD simulation. In order to overcome this problem and to explore the reaction paths of unexpected possible events, we exploit metadynamics[21] in the extended Lagrangean form[22,30] as implemented in the CPMD (www.cpmd.org) code.[29] This method consists of applying a history-dependent potential in the space of few collective variables (CVs), which are functions of the atomic coordinates and are able to describe the activated process of interest. The dynamics in the space of the CVs is coupled to the dynamics of the microscopic system and is biased by the history-dependent potential that is made of Gaussians centered on the trajectory of the CVs with a suitable width and height. The biasing potential helps to overcome the local minima of the free-energy surface (FES), forcing the system to explore the relevant parts of the coarse-grained space defined by the CVs. The sum of the Gaussians provides an estimate of the FES with an accuracy, which depends on the dimensionality of the CV space, their diffusion coefficient, and the parameters of the history-dependent potential.[30]

Several simulations have been carried out, employing two types of CVs, interatomic distances and coordination numbers. The use of distances as collective variables provides a fast and accurate estimate of the free-energy barriers along a predetermined reaction path. The coordination numbers are defined by means of sums of rational functions. The functional form and the details of the use of these CVs are reported in the literature.[22,23] The use of general collective variables (CVs), such as coordination numbers (CN), in metadynamics improves the predictive power of the method, allowing for unexpected paths to be found. Nevertheless, higher accuracy can be achieved when interatomic distances are used as CVs.[23]

The width of the Gaussians, placed every 10.0−12.0 fs, is chosen as one-fifth of the amplitude of the fluctuations in the related CV at the equilibrium, and the height is set to 1.25 kcal/mol, which is much smaller than the height of the potential energy barriers estimated in previous works.[18,31] We define two distances as CVs, namely, between H and O across the octahedral hole (D1), to which we associate a Gaussian width of 0.4 Å, and between H and O, which lie on the same $Al(OH)_2Al$ site (D2), associated with a Gaussian width of 0.2 Å (Figure 1a). We use different coordination numbers as CVs, the CN of the Al cation with respect to the O atoms of the OH groups with a width of 0.03 (CN1), the CN of the H atom with the O atoms which form the water molecule with a width of 0.01 (CN2), and the CN of the apical O atoms with the H atoms with a width of 0.01 (CN3). The parameters of the Gaussians that form the history-dependent potential have been chosen so as to reproduce the free-energy surface with an accuracy of 2

kcal/mol.

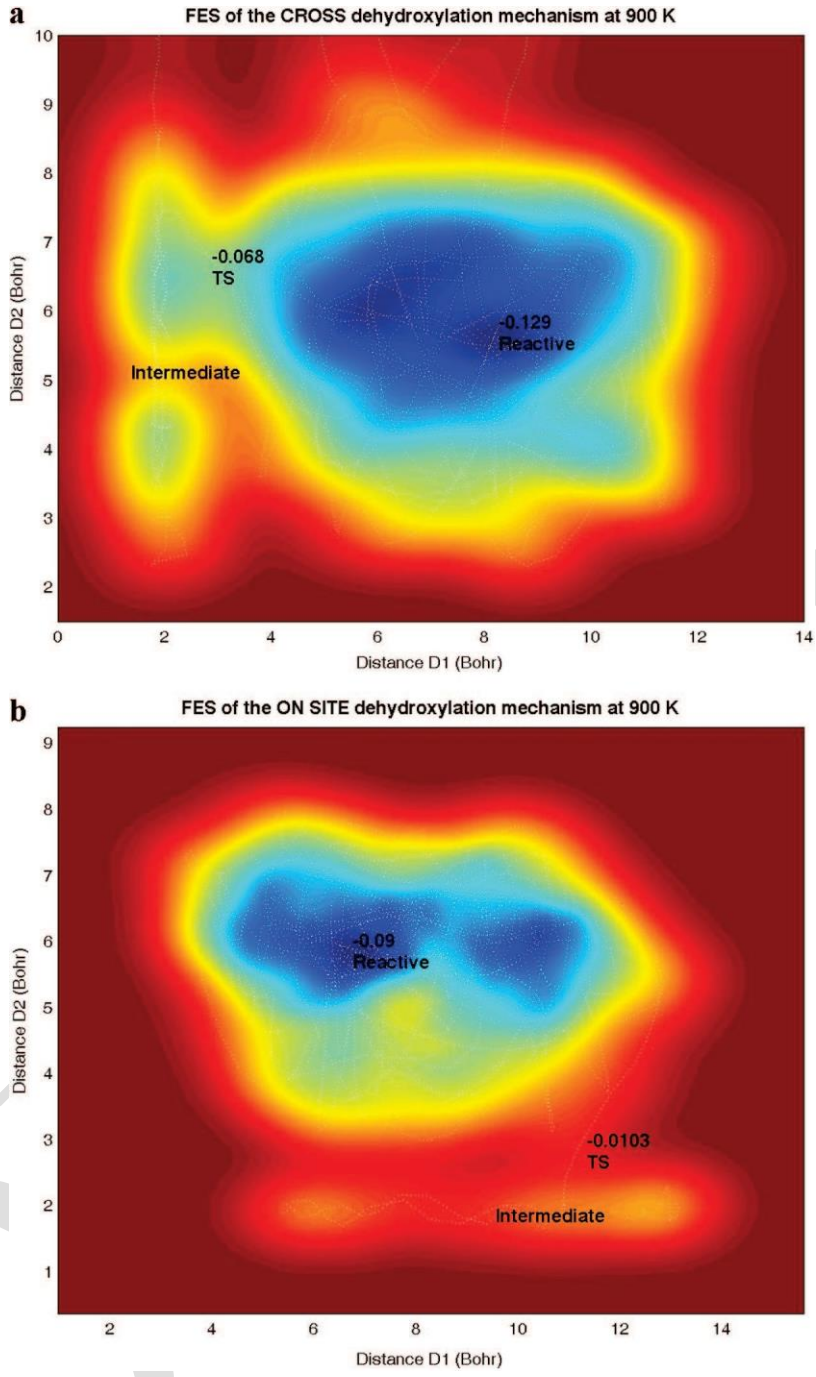

Figure 2. Free-energy surface as a function of the collective variables (CVs) for the cross (a) and on-site (b) mechanisms of dehydroxylation at 900 K (using interatomic distances as CVs). The free energy (Hartrees) is plotted against D1 and D2 by means of isoenergetic curves with a color profile from blue (lowest energy) to dark red (highest value).

The simulations are carried out starting from the initial structure of pyrophyllite and its cell parameters as determined experimentally by Wardle et al.[6] Before switching on the metadynamics, the system is equilibrated at the temperature of interest for 1.6 ps. During the equilibration runs, no chemical reaction is observed. The metadynamics run is continued until the reaction is achieved. When the dynamical reaction trajectories are identified, we explore the topology of the free-energy surface (FES) and analyze the structures in the minima and at the saddle points. We perform a full optimization of reactants and products, and the transition states (TS) are optimized by the PRFO algorithm at zero temperature, as implemented in the CPMD code.[32] The critical points are confirmed with calculations of harmonic frequencies by means of vibrational analysis through atomic finite displacements searching for no imaginary frequency for minimum-energy structures and one imaginary frequency for the TS.

Results and Discussion

At first, we assume that dehydroxylation occurs via the two possible mechanisms previously reported, namely, the cross and on-site mechanism. We performed simulations at two temperatures, 900 K and 1500 K, to understand the different behavior in the two temperature ranges and compare to experiments.[7]

We choose this upper limit of the temperature range, higher than the experimental one. The study has initially been performed in one unit cell and later extended to a 2 1 1 supercell, both with the application of the periodic boundary conditions. In the last part of this section, we explore the secondstep of the reaction where the high-temperature behavior is assumed to be due to the higher stability of the remaining OHsin the structure after the gradual loss of water.

Dehydroxylation Reaction. The set of simulations presented in this section are carried out in an unit cell that contains four complete aluminum octahedrons joined in pairs by hydroxyl groups. This number of hydroxyl groups is large enough to allow the reaction to occur via both mechanisms. The four hydroxyl groups that can be involved in the proposed mechanisms are shown in Figure 1a. In the initial structure, the distance between the oxygen atom and the hydrogen atom of the adjacent hydroxyl group (on-site distance) is 3.24 Å, and the one between the H atom of a hydroxyl group and the oxygen atom of the nearest hydroxyl group through the octahedral vacancy (cross distance) is 3.85 Å. Although the cross distance is larger than the on-site one, we observed during MD simulations of 360 fs that both distances can reach similar minimum values at 900 K (2.66 Å on-site distance and 2.86 Å cross distance), while at 1500 K, the minimum on-site (OH ⋯ O) distance is much shorter (2.19 Å) than the minimum cross distance (about 2.7 Å). This shorter(OH ⋯ O) distance could indicate an easier protonation via the on-site rather than the cross mechanism at high temperature. However, the rearrangement of the oxygen atoms of the hydroxyl groups and the reorientation of the hydroxyl bonds are necessary for the protonation, and the protonation of hydroxyl groups in the cross mechanism is less sterically hindered.

We applied metadynamics at 900 and 1500 K using as CVs the interatomic distances described above (D1 and D2 in Figure 1a) between the H and O atoms that participate in the water formation for the cross and on-site mechanisms. Both mechanisms were simulated, and the free-energy surfaces (FES) were reconstructed from the history-dependent biasing potential. The free-energy surfaces obtained in this manner show two minima and a saddle point that correspond, respectively, to the reactants, products, and the transition state of each mechanism (Figure 2). The product of this initial stage of dehydroxylation is a semidehydroxylated intermediate, that is, only two OH groups in the unit cell have reacted to produce a single water molecule. The fluctuation of the interatomic distances D1 and D2 in the minima is broad due to the large thermal mobility of the hydroxyl groups. In the cross mechanism, one hydrogen atom detaches from the oxygen atom and reaches the center of the octahedral hole toward the front OH group to form the transition state yielding a water molecule as a product (Figure 2a). During the metadynamics simulation, this distance H ⋯ OH becomes gradually shorter until binding occurs with an abrupt jump of D1 (Figure 3a). In the on-site mechanism (Figure 2b), the H atom jumps to the adjacent OH group in the same octahedral edge and forms the transition state. Afterward, the water molecule is produced with a decrease of D2 (Figure 3b). The total energy profiles at 0 K obtained from the optimization of the critical points of the reaction paths are represented in Figure 4. Total energies at 0 K of the reactant, transition states, intermediates, and products are shown in Table 1. The activation energy at 0 K of the on-site mechanism is only 0.9 kcal/mol higher than that of the cross mechanism (58.8 kcal/mol), which is consistent with the one reported for the protonation of the adjacent hydroxyl group for the on-site mechanism in a previous

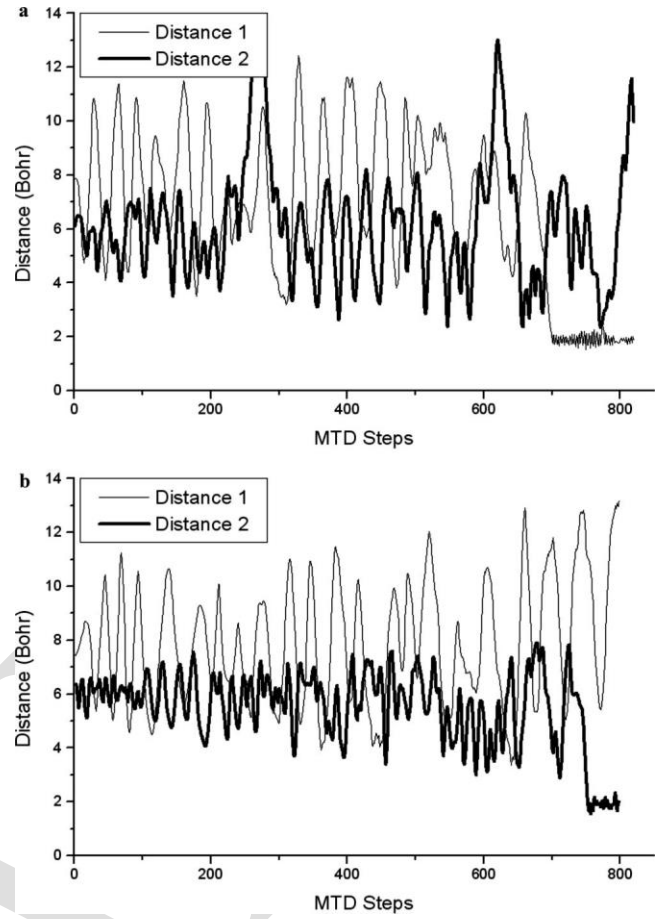

Figure 3. Evolution of the distances as collective variables during the metadynamics (MTD) at 900 K for the cross (a) and on-site (b) mechanisms.

work[18] and determined experimentally in montmorillonite.[34] Therefore, at low temperature, both processes are competitive. Upon raising the temperature to 900 K, the free-energy barrier for the cross mechanism (38.3 kcal/mol) becomes much lower than that for the on-site process (49.9 kcal/mol), revealing that the cross mechanism is favored at higher temperatures and the height of the free-energy barriers is very much affected by the entropic term. At 1500 K, the free-energy barriers for the cross and on-site mechanisms decrease to 36.6 and 45.8 kcal/mol, respectively (Table 2). The semidehydroxylate intermediate of the cross mechanism is 9.2 kcal/mol less stable than that obtained from the on-site mechanism (Table 1), and it would be more reactive for complete dehydroxylation than that of the on-site mechanism, especially at high temperatures. This difference of stability could be mainly attributed to the remaining $Al^{3+}-O-Al^{3+}$ group coming from the on-site mechanism, with respect to $Al^{3+}-OH-Al^{3+}$ group coming from the cross mechanism. Both semidehydroxylated structures obtained as products of this first step of the reaction display a water molecule located in the octahedral hole. During the simulation, the water molecule rotates in the hole and forms H bonds with the structural oxygen atoms. This intermediate is rather stable, and the complete dehydroxylation is not likely to proceed spontaneously because the migration of the water molecule to the interlayer space is hindered by the steric repulsion with the lone pairs of the basal oxygen atoms. While this water molecule is trapped in the octahedral hole, the reaction between the other two hydroxyl groups is inhibited. We have extended the exploration of the reaction mechanisms using coordination numbers as CVs, namely, the CN of the aluminum atoms with respect to the oxygens of the OH groups involved in the

formation of the water molecule (CN1) and the CN of the hydrogen atoms involved in the cross or on-site mechanism with respective oxygen counterparts in the water formation (CN2). For the cross mechanism, the topology of the FES with respect to the CVs shows two minima connected by a saddle point at 900 and 1500 K. The estimated free-energy barrier at 1500 K is 38.7 kcal/mol, which is similar to that obtained with interatomic distances as CVs.

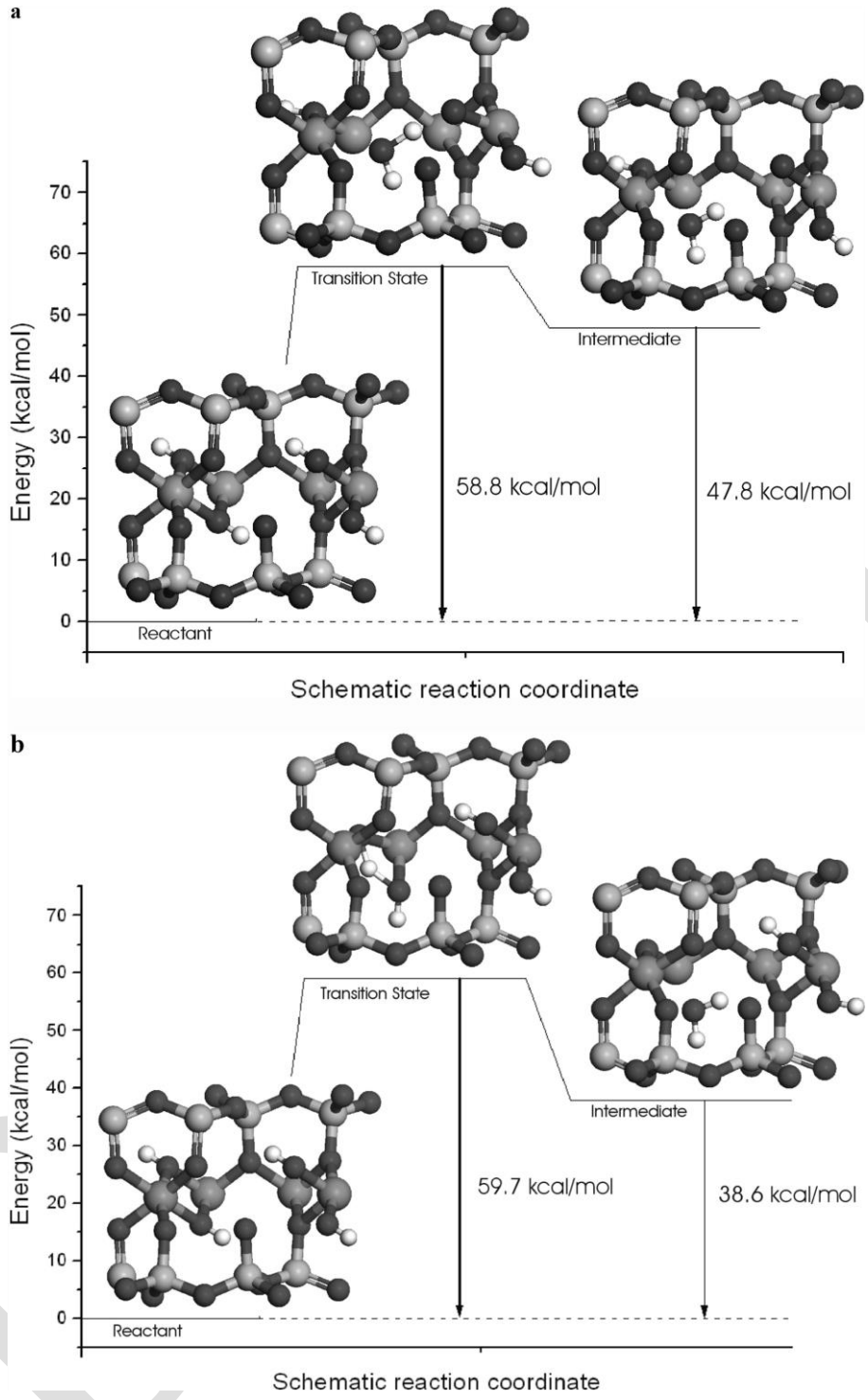

Figure 4. Reaction paths for the cross (a) and on-site (b) mechanisms for the dehydroxylation of pyrophyllite. The Al, Si, O, and H atoms are represented in dark grey, clear grey, black, and white colors, respectively.

Similar results were observed for the on-site mechanism. The free-energy (ΔG) estimation at 900 K for the on-site mechanism (51.5 kcal/mol) is consistent with the one obtained with interatomic distances as CVs (49.9 kcal/mol). Similar coincidence is observed at 1500 K, where the ΔG estimation is 47.8 kcal/mol (Table 2). It is worth noting that we have encountered a significant discrepancy only in the estimate of the free-energy barrier for the cross mechanism at 900 K (see Table 2), while for the other reaction paths, the values of ΔG correspond within the expected accuracy of the method. However, even in this less favorable case, the transition path is qualitatively similar to the one obtained using distances as CVs.

TABLE 1: Energies (at 0° K) of the Reactant, Intermediates, and Transition States of the Dehydroxylation Reactions of Pyrophyllite Optimized with Fixed Experimental Lattice Parameters of Pyrophyllite

structures	energy (Hartrees)	ΔE (kcal/mol)[a]
Intermediates		
1) pyrophyllite	−426.91185395	
2) on-site semidehydroxylate with water	−426.85029457	38.6 (2−1)
3) on-site semidehydroxylate without water	−409.73975733	
4) cross semidehydroxylate with water	−426.83568249	47.8 (4−1)
		9.2 (4−2)
5) cross semidehydroxylate without water	−409.69489083	41.2 (5−3)
6) dehydroxylate with water	−409.67159260	28.1 (6−3)
		14.6 (6−5)
7) dehydroxylate with water[b]	−409.68878177	
8) dehydroxylate without water[b]	−392.58526724	
9) first intermediate protonated in apical oxygen for on-site mechanism	−426.80158106	69.2 (9−1)
		30.6 (9−2)
10) first intermediate protonated in apical oxygen for cross mechanism	−426.84643473	41.0 (10−1)
		28.1 (9−10)
		6.7 (4−10)
		2.4 (10−2)
11) on-site semidehydroxylate without water[b]	−409.74739102	36.8 (7−11)
12) water[b]	−17.14341802	
Transition States (TS)		
13) on-site mechanism	−426.81665432	59.7 (13−1)
14) cross mechanism	−426.81807349	58.8 (14−1)
15) second step of on-site mechanism	−409.63842827	63.6 (15−3)
16) second step of on-site mechanism[b]	−409.65134004	60.3 (16−11)
17) on-site with apical oxygen I	−426.78783380	77.8 (17−1)
18) on-site with apical oxygen II	−426.79186241	75.3 (18−1)
19) cross with apical oxygen I	−426.84536236	41.7 (19−1)
20) cross with apical oxygen I	−426.80629564	66.2 (20−1)

[a] Energy differences between the structures whose numbers are indicated in brackets. [b] With the experimental lattice cell of dehydroxylate.

Participation of the Tetrahedral Apical Oxygens. Exploring the above-mentioned dehydroxylation mechanisms, we observed unexpected protonations of the surrounding structural apical oxygens. Then, we included a third CV accounting for the coordination of these apical oxygens with the H atoms (CN3) in the structure. Our simulations suggest the viability of a dehydroxylation mechanism across the octahedral hole that involves the assistance of the apical oxygen only at high temperature (1500 K). When the protonation of an apical oxygen is involved, the dehydroxylation turns into a two-step process

TABLE 2: Free Energy (kcal/mol) for the Reactions Simulated with Different Metadynamics Designs (For the Cross (X) and On-Site (OS) Mechanisms with Distances (*D*) and Coordination Numbers (CN) as CVs)

		OS		X	
reaction	CV	900 K	1500 K	900 K	1500 K
dehydroxylation	D1, D2	49.9	45.8	38.3	36.6
1st step dehydroxylation 1st step	CN1, CN2	51.5	47.8	48.3	38.7
dehydroxylation 1st step	CN1, CN2, CN3	58.8	52.4	49.6	42.7
assistance of apical oxygen	CN1, CN2, CN3				44.0
2nd step of dehydroxylation	D1, CN3	30.9	29.0		

The reaction path has been reconstructed at 0 K (Figure 5) by geometry optimization and transition-state search. The first step consists of the protonation of one apical oxygen, and afterward, the proton is transferred to the adjacent OH group. The associated activation energy at 0 K for the apical oxygen atom protonation is 41.7 kcal/mol, and it is 25.2 kcal/mol for the subsequent protonation toward the hydroxyl group. This means that the transition by this two-step mechanism is energetically disfavored (ΔH) 66.9 kcal/mol) with respect to the straightforward cross mechanism (ΔH) 58.8 kcal/mol, Figure 4) and explains why this mechanism is not likely to occur at low temperatures.

At 900 K, the protonation of the apical oxygens is detected; however, these protonated apical oxygens do not contribute to form a water molecule, and they deprotonate to the initial state. Nevertheless, even when a CV involving the protonation of the apical oxygens is included in the metadynamics scheme, the dehydroxylation follows the direct cross or on-site mechanisms without the assistance of the apical oxygens. The values of the free-energy barrier obtained in these simulations with CN as the CV are higher than those obtained when interatomic distances are used, although the trajectories and the main featuresof the FES are reproduced at least qualitatively.

The free-energy barriers to protonate the apical oxygens are, in general, low and sensitive to the temperature. However, although the protonation of a random apical oxygen is easy, the second step is only viable when the suitable apical oxygen with the protonated apical oxygen as an intermediate. Accordingly, the FES displays three minima connected by two saddle points of 42.9 and 2.1 kcal/mol with a global ΔG of 44 kcal/ mol (Table 2). This value is slightly higher than that obtained for the direct cross mechanism at 1500 K and comparable to the free-energy barrier for the direct on-site mechanism. This suggests that the two-step process would be a viable reaction channel at high temperature, even though it is not the main one.

is protonated, which is rarely the case when the reaction involves hydroxyl groups located on the same site. For this reason, many simulations with these CVs (CN1, CN2, and CN3) at 1500 K for the on-site mechanism yielded the direct mechanism, and only few of them showed the assistance of the apical oxygens. Here, we analyze the MD trajectory of the on-site mechanism with the assistance of apical oxygens. The reaction profile at 0 K (Figure 6) shows a first step of silanol formation with a barrier of 77.8 kcal/mol and a second step of water formation with a barrier of 6.1 kcal/mol. The silanol intermediate has a much higher total energy (69.2 kcal/mol with respect to pyrophyllite) than that of the homologous cross mechanism (41.05 kcal/mol related to pyrophyllite). This accounts for the low probability of this mechanism. Hence, the activation energy for this on- site mechanism with the apical oxygen assistance is higher (77.8 kcal/mol) than that of the homologous cross mechanism (66.9 kcal/mol) and than that of the straightforward on-site mechanism(59.7 kcal/mol).

In turn, the protonation of the apical oxygen becomes important at very high temperature, and it is the first stage before amorphization or melting occur. To verify this, a standard MD run has been performed with a $2 \times 1 \times 1$ supercell heated up

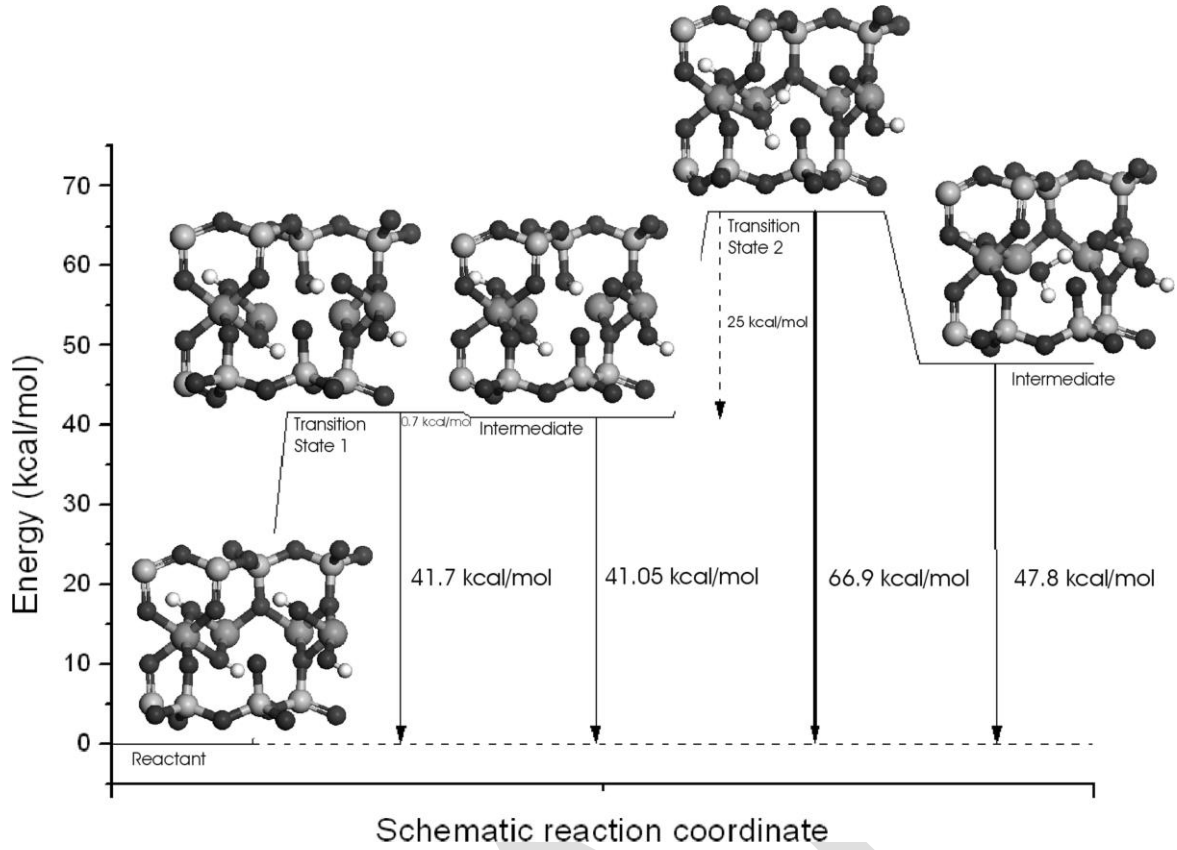

Figure 5. Reaction path for the cross mechanism with the assistance of apical O atoms. The Al, Si, O, and H atoms are represented in dark grey, clear grey, black, and white colors, respectively.

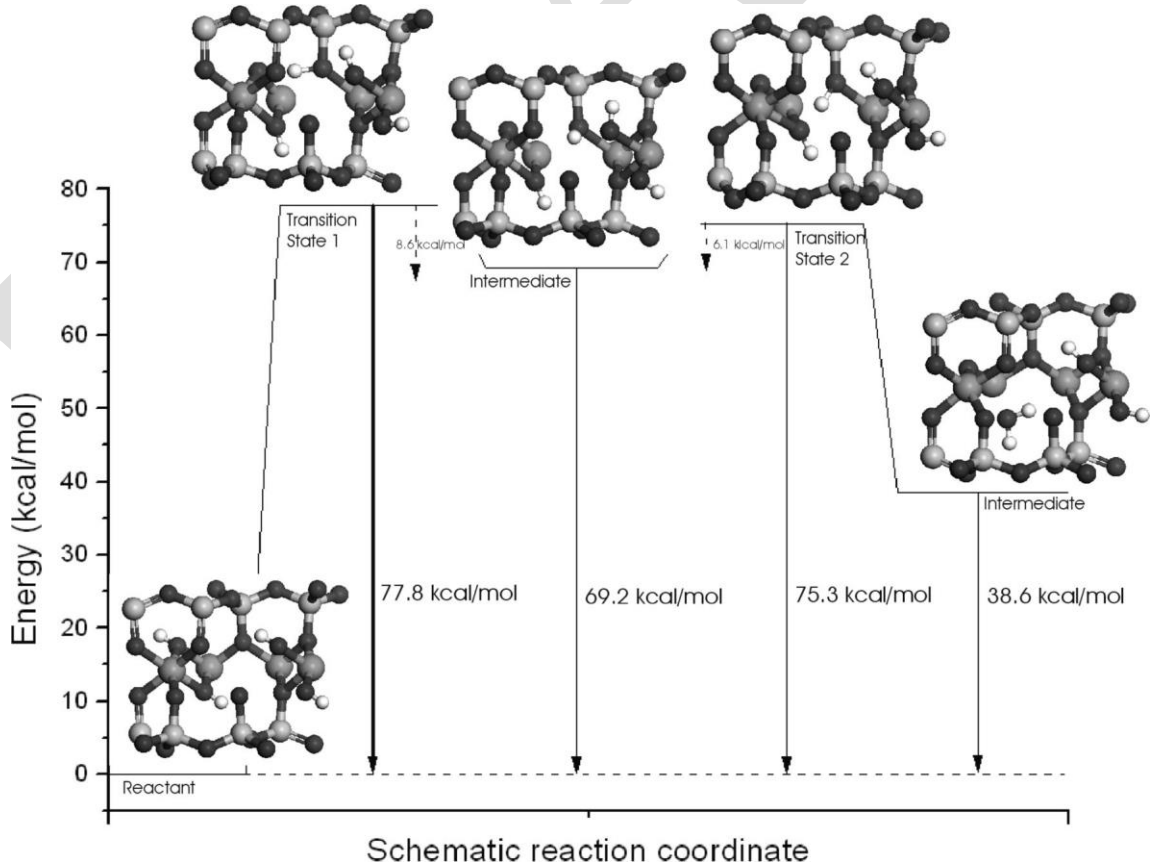

Figure 6. Reaction path for the on-site mechanism with the assistance of apical O atoms. The Al, Si, O, and H atoms are represented in dark grey, clear grey, black and white colors, respectively.

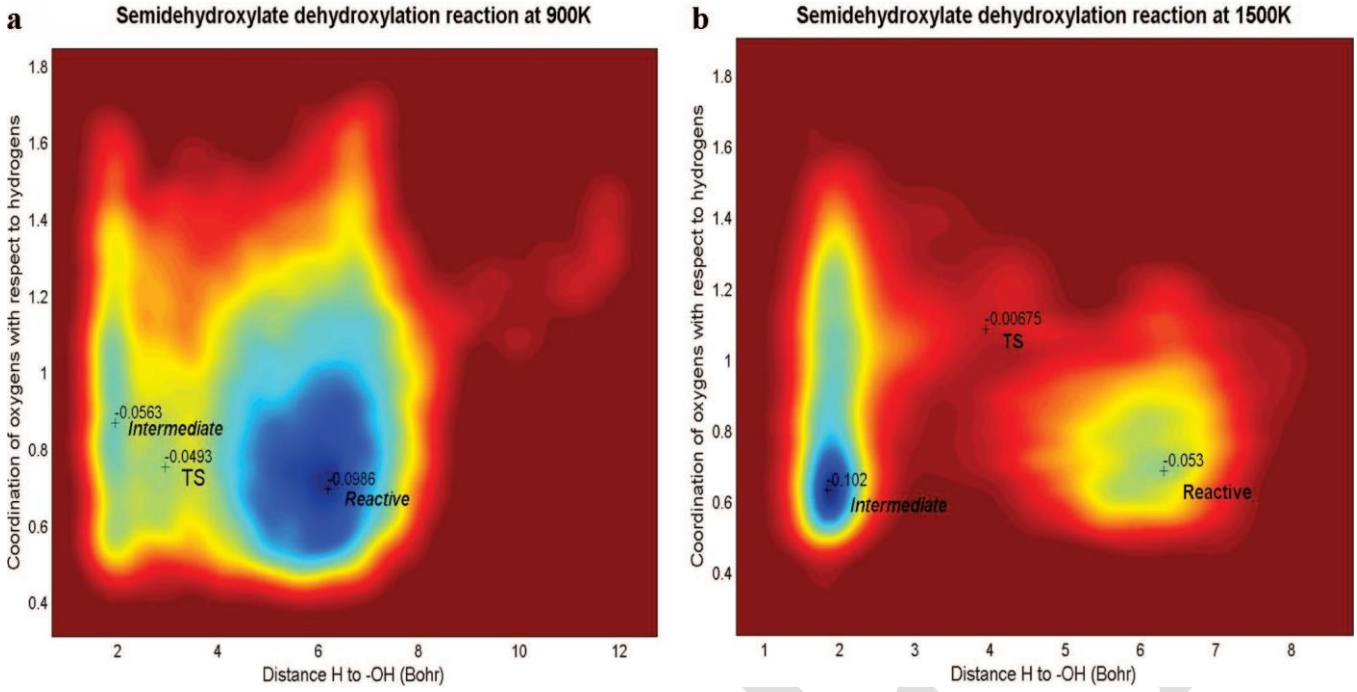

Figure 7. Free-energy surface of the second step of on-site dehydroxylation (from semidehydroxylate to dehydroxylate pyrophyllite) at 900 (a) and 1500 K (b). The free energy (Hartrees) is plotted against the CV by means of isoenergetic curves with a colour profile from blue (lowest energy) until dark red (highest value).

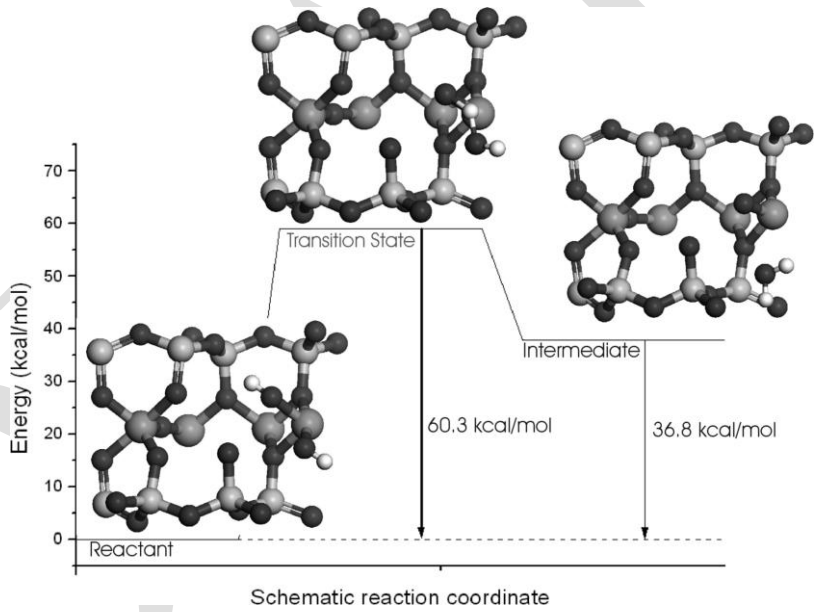

Figure 8. Reaction path of the second step on-site dehydroxylation on the semidehydroxylate derivative. The Al, Si, O, and H atoms are represented in dark grey, clear grey, black, and white colors, respectively.

to 3500 K to approach the point of mechanical instability. In this run of 0.6 ps, several protonations of the apical oxygens are observed before the system melts, but melting occurs beforeany water molecule is formed.

The Cross "Chain" Mechanism in a Larger Supercell. One of the characteristics predicted for the cross mechanism is the concerted character of bond exchange along chains. This chain mechanism cannot be simulated in the unit cell. Therefore, in order to elucidate the concerted mechanism and to rule out possible size effects from the results reported above, we have replicated the unit cell in the *a* direction. This 2 × 1 × 1 supercell incorporates two complete octahedral holes where the cross mechanism can take place and propagate along the chain of hydroxyl groups. We applied the metadynamics with the previous CNs as CVs (CN1, CN2, and CN3) for the cross mechanism at 1500 K. No concerted chain mechanism was observed, and only the formation of one water molecule was detected in one octahedral hole. Going further along with the metadynamic simulation, no additional water molecule was formed. This supports the hypothesis that the water moleculein the tetrahedral hole inhibits the chain reaction and that the complete release of water is necessary to achieve the complete dehydroxylation. This reaction follows the cross mechanism with the assistance of apical oxygens with a free-energy barrier of 26 kcal/mol. This would indicate that the cross mechanism tendsto progress more likely with the assistance of apical oxygens, whereas the on-site mechanism would follow the direct way.

Complete Dehydroxylation of the Semidehydroxylate. Previous experimental[7,8,13]and theoretical studies[14] indicate that the dehydroxylation reaction happens at least in two steps with the presence of intermediates. The semidehydroxylate derivatives found in this work for all mechanisms of the previous steps are the intermediates of the dehydroxylation process of pyrophyllite. After simulating the formation of the semidehydroxylate intermediates by reaction of the remaining OH groups in the unit cell, we now explore the complete dehydroxylation of the intermediate. We argue that the release of the previously formed water molecule is required for the further reaction process. In fact, we observe that while the water molecule remains in the octahedral hole, no other attempt to proceed to the complete dehydroxylation yields success. We have computed the energy produced by the release of the water molecule as

$$\Delta E = -(E(\text{dehydrated intermediate}) + E(H_2O) - E(\text{dehydroxylated intermediate}))$$

which is defined positive when the reaction is exothermic (Table 1). The ΔE for the dehydration of the intermediate from the on-site reaction is 20.6 kcal/mol, which is consistent with previous DFT studies.[14] The energy released from the dehydra-tion of the cross mechanism intermediate is much smaller (1.65kcal/mol) due to the high energy of the semidehydroxylate intermediate in this mechanism (Table 1), and Stackhouse et al.[18] found an energy requirement of about 12 kcal/mol for the complete water release in DFT calculations on pyrophyllite dehydroxylation. This energy is much lower than those related to the dehydroxylation processes discussed above; thus, we arguethat the release of the water molecule is not the rate-limiting step of the whole dehydration process of pyrophyllite.

Hereafter, we will investigate the dehydroxylation of the semidehydroxylate derivative assuming that the water molecule from the previous dehydroxylation has already been released. We perform metadynamics simulations at 900 and 1500 K with two CVs: the distance from the −OH hydrogen to the contiguous −OH group (D2) and the coordination of the apical oxygens with the hydrogen atoms (CN3). The FES as a function of the CVs shows two basins of stability connected by a single transition state at both temperatures (Figure 7). Our simulations indicate that the second step of the dehydroxylation occurs by crossing a free-energy barrier of 29.0 kcal/mol at 900 K and 30.9 kcal/mol at 1500 K. These critical points were fully optimized at 0 K, resulting in an enthalpy barrier of 60.3 kcal/mol (Figure 8). In this calculation, we use the experimental cell parameters for the dehydroxylate derivative, as determined elsewhere.[33] This barrier is similar to that of the first step of reaction, 59.7 kcal/mol (see Figure 4b).

Guggenheim et al.[8] interpreted their experimental results, arguing that with the water loss from some OH groups in the partially dehydroxylated system, certain domains of the structure contain five-fold aluminum coordination, and the Al−OH bonds of the remaining OH groups become stronger and will have a different activation energy for the total dehydroxylation from that of the original OH species in the pyrophyllite structure, and a higher temperature is needed for the next water molecule formation. However, we find that the free-energy barrier of the second step is lower than that of the first step (Table 2), and the activation energy at 0 K is similar for both steps of dehydroxylation (59.7 and 60.3 kcal/mol). A similar result was found by Stackhouse et al.,[18] who estimate an activation energy for this reaction as 56.2 kcal/mol.

The release of water in the dehydroxylate product is also exothermic, with an energy of 25 kcal/mol that is consistent with previous DFT calculations for the reaction.[14]

When the cross semidehydroxylate intermediate without water is used as the reactant for the second dehydroxylation reaction step, we observe that it evolves to the on-site semidehydroxylate intermediate by the assistance of apical oxygens, and no water molecules are formed. This exchange to the on-site intermediate is certainly strengthened because of its higher stability (41.2 kcal/mol) with respect to the cross intermediate (Table 1). Nonetheless, this aspect needs further investigations.

Conclusions

The application of ab initio molecular dynamics along with metadynamics allows us to reproduce the dehydroxylation of pyrophyllite, finding new intermediates, establishing the possible mechanisms, and evaluating the energetics of this reaction.

The first step of dehydroxylation generates semidehydroxylate intermediates characterized by the presence of a water molecule in the octahedral hole, five-fold coordination for the Al^{3+} pairs implicated in the reaction, and a residual oxygen (O) under-saturated with respect to positive charge because of the hydroxyl group loss. The dehydroxylation process produces different intermediate semidehydroxylated structures with different binding energies. Both dehydroxylation mechanisms previously proposed, cross and on-site, are viable and competitive with a similar activation energy at low temperature, with the cross mechanism having a lower free-energy barrier.

At high temperature (1500 K), the cross mechanism becomes predominant, and the dehydroxylation mechanism may involve the apical structural oxygens in a competitive two-stage cross mechanism. The intermediate for these processes is constituted by the protonated apical oxygen, which is the only one able to transfer again the proton to the OH group, leading to the formation of water. However, this apical oxygen assistance does not decrease the free energy. The free energy of the cross mechanism with this assistance is similar to that without this assistance.

Our simulations in a large supercell also show that the release of the water molecule formed in the first step of the dehydroxylation is necessary for the progress of the complete dehydroxylation, thus ruling out the possibility of a concerted chain effect related to the cross mechanism. In turn, due to its lower stability, the intermediate of the cross mechanism is most likely to transform into the semidehydroxylate obtained from the on- site process, even though the complete cross dehydroxylation mechanism is still under study.

The calculated activation energy of the total dehydroxylation (59.7−60.3 kcal/mol) is consistent with that found experimentally in montmorillonite (59.8 kcal/mol).[34] The activation energy of the partial dehydroxylation is identical to that of the total dehydroxylation, and the free energy of the total dehydroxylation is lower than that of the first step of dehydroxylation. This behavior can be extended at least to the rest of the dioctahedral 2:1 phyllosilicates.

Acknowledgment. The authors are thankful to the Centro Técnico de Informática of CSIC, Centro de Cálculo del CIEMAT, Centro de Cálculo de Galicia (CESGA), and the Centro de Supercomputación de la Universidad de Granada for allowing the use of its computational facilities. E. Molina-Montes is thankful to MEC for financial support within the FPU programme. This work was supported by Spanish MCYT an

European FEDER Grants BTE2002-03838, CGL2005-02681, and CTQ2004-04648.

References and Notes

(1) Bruce, C. H. *AAPG Bull.* **1984**, *68*, 673.
(2) Burst, J. F. *Ann. Re*V. *Earth Planet. Sci.* **1976**, *4*, 293.
(3) Velde, B.; Vasseur, G. *Am. Mineral.* **1992**, *77*, 967.
(4) Grim, R. E.; Bradley, W. F. *J. Am. Ceram. Soc.* **1940**, *23*, 242.
(5) Fitzgerald, J. J.; Hamza, A. I.; Dec, S. F.; Bronnimann, C. E. *J. Phys. Chem.* **1996**, *100*, 17351.
(6) Wardle, R.; Brindley, G. W. *Am. Mineral.* **1972**, *57*, 732.
(7) Wang, L.; Zhang, M.; Redfern, S. A. T.; Zhang, Z. *Clays Clay Miner.* **2002**, *50*, 272.
(8) Guggenheim, S.; Chang, Y. H.; Koster van Gross, A. F. *Am. Mineral.* **1987**, *72*, 537.
(9) Drits, V. A.; Besson, G.; Muller, F. *Clays Clay Miner.* **1995**, *43*, 718.
(10) McKenzie, K. J. D.; Brown, I. W. M.; Meinhold, R. H.; Bowden, M. E. *J. Am. Ceram. Soc.* **1985**, *68*, 266.
(11) Ogloza, A. A.; Malhotra, V. M. *Phys. Chem. Miner.* **1989**, *16*, 378.
(12) Malhotra, V. M.; Ogloza, A. A. *Phys. Chem. Miner.* **1989**, *16*, 386.
(13) Heller, L.; Farmer, V. C.; Mackenzie, R. C.; Mitchell, B. D.; Taylor, H. F. W. *Clay Miner. Bull.* **1962**, *5*, 56.
(14) Sainz-Díaz, C. I.; Escamilla-Roa, E.; Hernández-Laguna, A. *Am. Mineral.* **2004**, *89*, 1092.
(15) Kloprogge, J. T.; Kamarneni, S.; Yanagirawa, K.; Fry, R.; Frost, R. L. *J. Colloid Interface Sci.* **1999**, *212*, 562.
(16) Boek, E. S.; Sprik, M. *J. Phys. Chem. B* **2003**, *107*, 3251.
(17) Sainz-Díaz, C. I.; Timón, V.; Botella, V.; Artacho, E.; Hernández-Laguna, A. *Am. Mineral.* **2002**, *87*, 958.
(18) Stackhouse, S.; Coveney, P. V.; Benoit, D. M. *J. Phys. Chem. B* **2004**, *108*, 9685.
(19) Car, R.; Parrinello, M. *Phys. Re*V. *Lett.* **1985**, *55*, 2471.
(20) Tuckerman, M. E.; Martyna, G. I. J. *J. Phys. Chem. B* **2000**, *104*, 159.
(21) Laio, A.; Parrinello, M. *Proc. Natl. Acad. Sci. U.S.A.* **2002**, *99*, 12562.
(22) Iannuzzi, M.; Laio, A.; Parrinello, M. *Phys. Re*V. *Lett.* **2003**, *90*, 238.
(23) Churakov, S. V.; Iannuzzi, M.; Parrinello, M. *J. Phys. Chem. B* **2004**, *108*, 11567.
(24) Donadio, D.; Bernasconi, M. *Phys. Re*V. *B* **2005**, *71*, 073307.
(25) Kohn, W.; Sham, L. J. *Phys. Re*V. **1965**, *140*, 1133.
(26) Becke, A. D. *Phys. Re*V. *A* **1998**, *38*, 3098.
(27) Lee, C.; Yang, W.; Parr, G. M. *Phys. Re*V. *B* **1988**, *37*, 785.
(28) Troullier, N.; Martins, J. L. *Phys. Re*V. *B* **1991**, *43*, 1993.
(29) *CPMD*, version 3.9.2; IBM Corp., MPI fuer Festkoerperforschung Stuttgart: Stuttgart, Germany, 2004.
(30) Laio, A.; Rodriguez-Fortea, A.; Gervasio, F.; Ceccarelli, M.; Parrinello, M. *J. Phys. Chem. B* **2005**, *109*, 6676.
(31) Mazzucato, E.; Artioli, G.; Gualtieri, A. *Phys. Chem. Miner.* **1999**, *26*, 375.
(32) Billeter, S. R.; Curioni, A.; Andreoni, W. *Comput. Mater. Sci.* **2003**, *27*, 437.
(33) Lee, J. H.; Guggenheim, S. *Am. Mineral.* **1981**, *66*, 350.
(34) Bray, H. J.; Redfern, S. A. T. *Mineral. Mag.* **2000**, *64*, 337.